optica

Strong magneto-optical response enabled by quantum two-level systems:supplementary material

LEI YING,[1] MING ZHOU,[1] XIAOGUANG LUO,[2] JINGFENG LIU,[3] AND ZONGFU YU[1,*]

1. *Department of Electrical and Computer Engineering, University of Wisconsin, Madison, Wisconsin 53706, USA*
2. *Department of Physics, Southeast University, Nanjing 211189, China*
3. *College of Electronic Engineering, South China Agricultural University, Guangzhou 510642, China*

Published 20 September 2018

This document provides supplementary information to "Strong magneto-optical response enabled by quantum two-level systems," https://doi.org/10.1364/OPTICA.5.001156.

I. Traditional small MO nanoparticles

In this section, we discuss the magneto-optical (MO) effect of small nanoparticles made of conventional MO materials and transition metals. We show their MO response is much weaker than the proposed magnetized-nanoparticle composite.

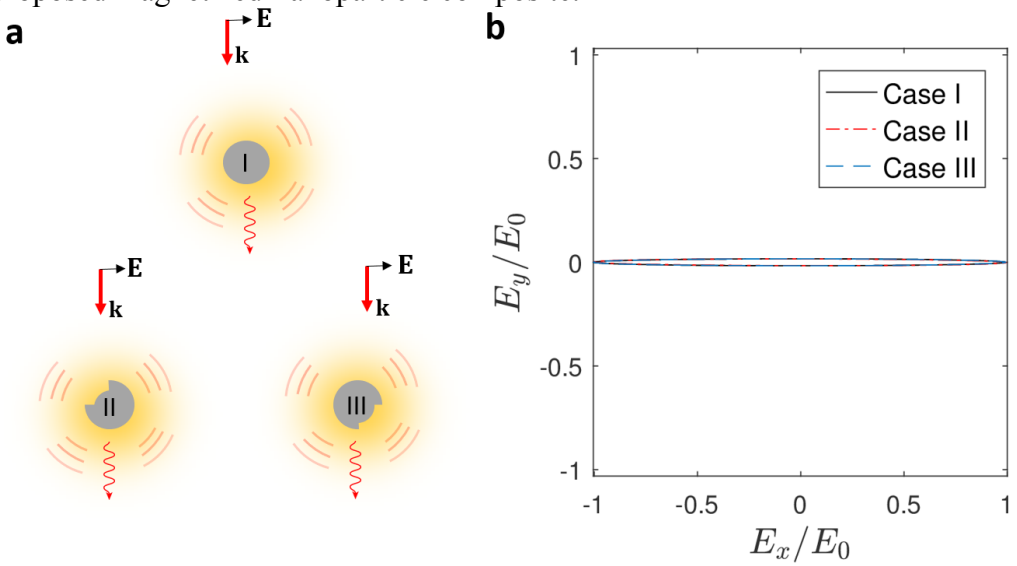

A. Scattering of small nanoparticles with different geometrical shapes

FIG. **S1** (a) Schematics of scattered fields for small MO nanoparticles with different geometrical shapes. They all have a size much smaller than the wavelength. The diagonal and off-diagonal elements of dielectric tensor are $\varepsilon_{xx} = 6.25$ and , $\varepsilon_{xy} = 0.06i$. (b) Polarizations of forward scattered fields for three cases in (a). The incident field is *x*-polarized.

At the deep sub-wavelength scale, i.e. size of nanoparticle $d \ll \lambda$, the geometrical shape of the object does not have significant impact on the scattering field. Here, we use full-wave simulation to show the polarization of forward scattered field for small MO particles with different geometrical shapes. As shown in Fig. S1, the forward scattered polarizations are almost identical.

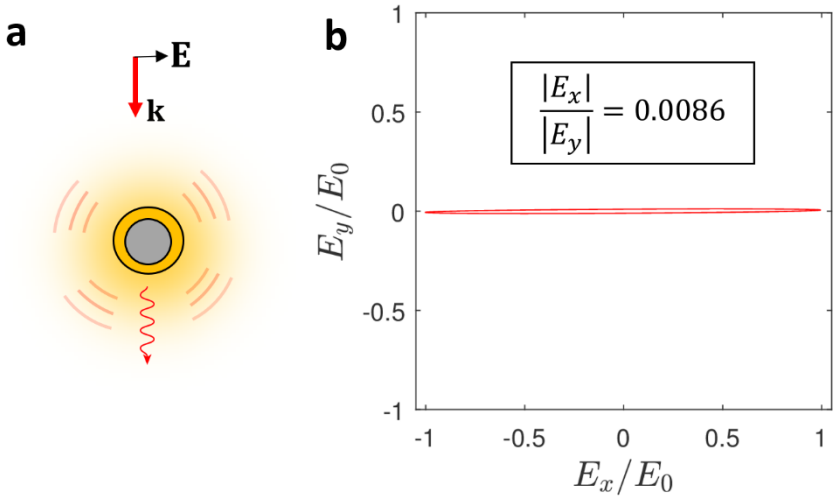

B. Gold-coated MO particle

FIG. S2 (a) Schematic of scattered field for a small Co-Au core-shell nanoparticle. The diagonal and off-diagonal elements of dielectric permittivity tensor are $\varepsilon_{xx} = -8.8 + 14.31i$ and , $\varepsilon_{xy} = 0.434 - 0.107i$ [4]. (b) Polarization of forward scattered field.

Previous work [2,3] used gold nanoparticles to enhance the MO effect of transition metals. Here we show that their MO responses are much weaker than the magnetized-nanoparticle composite. Here we consider a 10 nm Cobalt nanoparticle with a 5nm-thick gold shell. The polarization of the scattered field indicates the ratio of polarizability of the particle and the ratio is $|E_y|/|E_x| = 0.0086$, as shown in Fig. S2b. In the TLS-nanoparticle system, the ratio is almost 1, which is 2-3 orders of magnitude stronger than the Co-Au nanoparticle. We note that the metallic shell can enhance the MO strength by enhancing the local electric field of cobalt particles. However, strong absorption in Co or other transition metals significantly decrease the enhancement effect.

II. Weak MO response in large systems

Here we explain why one cannot use a super-large TLS or even solid material to realize strong MO response as demonstrated in main text.

A small TLS system supports an isolated transition, while a bulk material often has densely packed transitions in the energy spectrum. These dense transitions result in overlap of magnetized levels and, thus, MO response is weakened.

We start by explaining the MO effect in a small TLS, say a disk with a radius of 5 nm. As shown as case I in Fig. S3, only one pair of splitted levels are in an specific energy range, which are indicated by $|m = \pm 1\rangle$, where m is the magnetic quantum number. The Zeeman splitting energy is $\Delta E \sim |m|B$. Under a moderate magnetific field, e.g. 0.2T, the energy split can be much greater than the bandwidth of the transition. Then, the transitions $\sigma^{\pm}$ are well separated and they correspond to clock-wise (CW) and counter clock-wise (CCW) polarized light, respectively. It is important for CW and CCW transitions to be well separated to observe strong MO effect. When CW and CCW transitions perfectly overlap (i.e. no magnetic field), MO response vanishes. A small TLS with well separated energy levels can show maximum MO response.

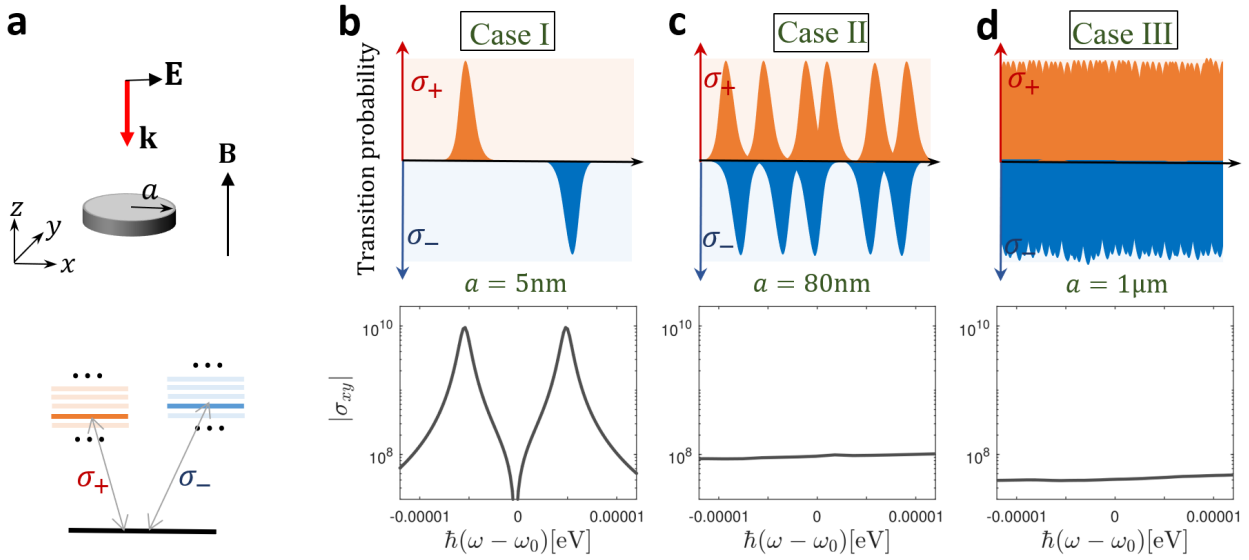

FIG. S3 (a) Upper: Schematic of a quantum volume illuminated by a x-polarized light with an external magnetic field **B**. Lower: Schematic of CW (σ^+) and CCW (σ^-) transitions . (b-d) Transition probability (upper) for and absolute conductivity $|\sigma_{xy}|$ (lower) versus frequency of a cylindrical quantum volume in microscopic ($a = 5\,\text{nm}$), mesoscropic ($a = 80\,\text{nm}$), and macroscopic ($a = 1\,\mu\text{m}$) scales, respectively. The magnetic field is $B_z = 0.2\text{T}$. For the upper figures, the horizontal and vertical axes indicate the transition frequency and the transition probability of CW and CCW transitions $\sigma^{\pm}$, respectively.

If the size of vlomum is large, e.g. tens or even hundreds of nanometers, there are a large number of energy levels in a specific energy range. In this case, the overlap between transtions $\sigma^{\pm}$ is inevitable. Due to the overlap between transitions $\sigma^{\pm}$, the overall MO response is signficantly weakened as shown in Fig. S3c.

In order to support the above understanding, we perform electrodynamic analysis of quantum dots with different sizes. We calculate the probability of transitions $\sigma^{\pm}$ and the off-diagnal optical conductivity $\sigma_{xy}(\omega)$ for a cylindrical disk with three sizes: radius $a = 5$nm, 80nm and 1μm, as shown in Figs. S3b-d, respectively. We consider semiconductor quantum dots. The effective masses of electrons and holes are $m_e = 0.13m_0$ and $m_h = 0.45m_0$, respectively. m_0 is the static mass of an electron in free space and the bandgap is $E_g = 1.751eV$. The energy-momentum relation of electrons and holes near bandgap is parabolic and given by $E \sim k^2$. Such a system is applied with a magnetic field $\mathbf{B} = [0,0,B]^T$ and its coresponding Zeeman splitting energy is given by $\Delta E = \frac{e\hbar}{2}\left(\frac{1}{m_e} + \frac{1}{m_h}\right)|m|B$ [4]. For example, with a magnetic field $B = 0.12$T, the Zeeman splitting energy is 1.3×10^{-4}eV. Note that if the Zeeman splitting is primary casused by spin, ΔE will be different and the Landé g-factor is important.

The MO response is extreme strong in quantum TLS, while relatively weak in large system or even bulk system. It can be characterized by the off-diagnal optical conductivity $\sigma_{xy}(\omega)$. For example, for the system with a radius $a = 5$nm, the Zeeman split is large enough that there is no overlap between transitions $\sigma^{\pm}$ and thus the optical conductivity shows strong MO response at the frequencies of transitions $\sigma^{\pm}$. However, for the large system (case III), strong overlapping effect emerges due to the dense transitions $\sigma^{\pm}$ and it results in weak MO response. The optical conductivity in Fig. S3d is two orders smaller than case I. For an intermediary case ($a = 80$nm), the density of transitions is countable and the overlapping effect is not serious as the macroscopic case. Thus the value of the off-diagonal optical conductiviry $|\sigma_{xy}(\omega)|$ is also intermediate between case I and case III.

The model to calculate the transition probability and the optical coductivity of a cylindrical disk is shown below. Since the magnetic field is normal to the disk surface, the Schrödinger equation can be written as

$$\widehat{H}\Psi = E\Psi,$$

$$\widehat{H} = \widehat{H}_{\perp} + \widehat{H}_{\parallel}, \quad \Psi = \phi_{\perp}\phi_{\parallel}, \quad E = E_{\perp} + E_{\parallel},$$

$$\widehat{H}_{\perp} = (\hbar^2/2m^*)\left[(\partial/\partial x - A_x)^2 + \left(\partial/\partial y - A_y\right)^2\right] + V_{\perp}(x,y), \tag{S1}$$

$$\widehat{H}_{\parallel} = (\hbar^2/2m^*)\partial^2/\partial x^2 + V_{\parallel}(z),$$

$$V_{\perp}(x,y), V_{\parallel}(z) = \begin{cases} 0, & \text{inside disk} \\ \pm\infty, & \text{others} \end{cases}.$$

Subscripts "∥" and "⊥" denote the directions being paralleled to and normal to the disk surface, respectively. m^* is the effective mass of electrons (m_e) or holes (m_h). Postive "+" and negive "-" potentials are applied to electrons and holes, respectively. The wavefunction and energy with subscript "∥" are analytical and they are given by $\phi_{\parallel}^n(z) = \sqrt{1/\pi\hbar}\sin(nz/2\hbar)$ and $E_{\parallel}^n = n^2\pi^2\hbar^2/2m^*$ ($n = 1,2,3\cdots$), respectively. Therefore, we just need to calculate a two-dimensional problem with a magnetic field. For numerically calculating the two-dimensional Schrödinger equation, we can discretetize on x-y plane. It is also called tight-binding model and the Hamiltonian is written as [5]

$$\widehat{H}_{\perp} = \sum_i \epsilon_i \hat{c}_i^{\dagger}\hat{c}_i + \sum_{\langle i,j \rangle} \left[t_{ij}\hat{c}_i^{\dagger}\hat{c}_j + \text{h.c.}\right], \tag{S2}$$

where $c_i^{\dagger}$and c_i are the creation and annihilation operators at ith site, respectively. ϵ_i is the on-site energy of ith site.

$$t_{ij} = \frac{\hbar^2}{2m^*\Delta a^2} e^{-e/\hbar \oint_C \mathbf{A}\cdot d\mathbf{r}} \tag{S3}$$

is the nearest neighbor hopping energy with a gauge field $\mathbf{A} = [-By/c, 0, 0]^T$. Δa is the square latteice constant. The eigenvalues and eigenvectors of Hamiltonian (S2) are the eigen energies and eigen wavefunctions on x-y plane with a hard boundary. Note that the eigen states from tight-binding approximation are only valid at low energy regime, i.e. $E_{\perp} < \hbar^2/(2m^*\Delta a^2)$.

Then, the optical conductivity $\sigma_{xy} = \sigma'_{xy} + i\sigma''_{xy}$ is given by [6, 7]

$$\sigma'_{xy} = A\sum_{\alpha\beta}\left[\frac{|\langle\beta|\pi^-|\alpha\rangle|^2}{\omega_{\beta\alpha} - \omega} - \frac{|\langle\beta|\pi^+|\alpha\rangle|^2}{\omega_{\beta\alpha} - \omega}\right],$$

$$\sigma_{xy}'' = A\sum_{\alpha\beta}\{|\langle\beta|\pi^-|\alpha\rangle|^2[\delta(\omega_{\beta\alpha}-\omega)+\delta(\omega_{\beta\alpha}+\omega)] \quad \text{(S4)}$$
$$-|\langle\beta|\pi^-|\alpha\rangle|^2[\delta(\omega_{\beta\alpha}-\omega)+\delta(\omega_{\beta\alpha}+\omega)]\},$$

where $A = ne^2/(\hbar m_e m_h V)$ and α, β are the lower and upper levels in a transition. We emphasize that, in some real bulk materials, the MO effect is more complicated and it is also contributed by the difference in density of ground states and in transition probabilities between σ^+ and σ^-[13].

III. Quantum electrodynamic modeling of magnetized TLS-nanoparticle composite

In this section, we describe the quantum electrodynamic modeling of the magnetized TLS-nanoparticle composite.

A. General formulism of the TLSs and nanostructure under magnetic field.

First, we consider a quantum-classical composite consiting of a single TLS and a single nanoparticle. Based on the quantization of the electromagnetic radiation in dispersive and absorptive inhomogeneous materials, the Hamiltonian is given by [8]

$$\widehat{H} = \int d^3r \int_0^\infty d\omega\left[\hbar\omega\hat{\mathbf{f}}^\dagger(\mathbf{r},\omega)\hat{\mathbf{f}}(\mathbf{r},\omega)\right]$$
$$+\sum_m\left[\frac{1}{2}\hbar\omega_m\hat{s}_m^{(z)} - \left(\boldsymbol{\mu}_m\cdot\hat{\mathbf{E}}^{(+)}\hat{s}_m + \hat{s}_m^{+}\boldsymbol{\mu}_m\cdot\hat{\mathbf{E}}^{(-)}\right)\right], \quad \text{(S5)}$$

where $\hat{\mathbf{f}}^\dagger(\mathbf{r},\omega)$, $\hat{\mathbf{f}}(\mathbf{r},\omega)$ are the bosonic vector field operators for the elementary excitations of the system. ω_α is the frequency of transition $|\text{ground}\rangle \to |m\rangle$ and $\hat{\sigma}_m^{(z)}$ is the population difference opteror for transition m. $m = \pm$ represent CW and CCW transitions, respectively. $\hat{s}_m$is the Pauli operator and $\boldsymbol{\mu}_m$ denotes the transition dipole moment. The electric field operator is expressed as $\hat{\mathbf{E}}^{(+)} = \mathbf{E}_0 + \mathbf{E}_0^s + \hat{\mathbf{E}}_s^{(+)}$ at the TLS position $\mathbf{r}_{\text{TLS}}$, where the first two terms are the electric field without TLS. Under the Markov approximation, the third term is given by [9]

$$\hat{\mathbf{E}}_s^{(+)}(\mathbf{r}) = \frac{\omega^2}{\varepsilon_0 c^2}\sum_m[\mathrm{P}\int_0^\infty d\omega\,\frac{\omega^2}{\pi\omega_L^2}\frac{\mathrm{Im}\overleftrightarrow{\mathbf{G}}(\mathbf{r},\mathbf{r}_{\text{TLS}},\omega)}{\omega-\omega_L} + i\mathrm{Im}\overleftrightarrow{\mathbf{G}}(\mathbf{r},\mathbf{r}_{\text{TLS}},\omega_L)]\cdot\boldsymbol{\mu}_m\,\hat{s}_m\,, \quad \text{(S6)}$$

where P and Im denote the principal value of the integral and imaginary part of a function, respectively. Then we use Heisenberg equations of motion and then calculate the traces of operators $\hat{s}_m$ and $\hat{s}_m^{(z)}$. As a result, the modified optical Bloch equations are obtained as

$$\begin{aligned} \langle \dot{\hat{S}}_m \rangle &= -\frac{\Gamma_m}{2}\langle \hat{S}_m \rangle - i\frac{\Omega_m}{2}\langle \hat{s}_m^{(z)} \rangle, \\ \langle \dot{\hat{s}}_m^{(z)} \rangle &= i\left(\Omega_m \langle \hat{S}_m{}^{\dagger} \rangle - \Omega_m^* \langle \hat{S}_m \rangle\right) - \Gamma_m\left(1 + \langle \hat{s}_m^{(z)} \rangle\right), \end{aligned} \tag{S7}$$

where $\hat{S}_m(t) = \hat{s}_m(t)e^{i\omega t}$. The detunning, the modified decay rate, and the complex Rabi frequency are respectively given by

$$\begin{aligned} \Delta_m &= \omega - \omega_0^m - \left(\frac{\omega^2}{\hbar\varepsilon_0 c^2}\right)\boldsymbol{\mu}_m^{\dagger} \cdot \mathrm{Re}\overleftrightarrow{\mathbf{K}}(\mathbf{r}_0, \mathbf{r}_0, \omega) \cdot \boldsymbol{\mu}_m, \\ \Gamma_m &= \left(\frac{2\omega^2}{\hbar\varepsilon_0 c^2}\right)\boldsymbol{\mu}_m{}^{\dagger} \cdot \mathrm{Im}\overleftrightarrow{\mathbf{G}}(\mathbf{r}_0, \mathbf{r}_0, \omega) \cdot \boldsymbol{\mu}_m, \\ \Omega_m &= 2\boldsymbol{\mu}_m{}^{\dagger} \cdot \frac{\mathbf{E}(\mathbf{r}_0)}{\hbar}. \end{aligned} \tag{S8}$$

The induced dipole moment can be solved from the above equation as

$$\mathbf{d}_m = \langle \hat{S}_m \rangle \boldsymbol{\mu}_m = \frac{-\boldsymbol{\mu}_m \Omega_m (2\Delta_m - i\Gamma_m)}{4\Delta_m{}^2 + 2|\Omega_m|^2 + \Gamma_m{}^2}. \tag{S9}$$

In the weak field limit, the second-order term $|\Omega_m|^2 \to 0$ and thus the induced dipole moment can be written as

$$\mathbf{d}_m \approx \frac{-\boldsymbol{\mu}_m \Omega_m}{2\Delta_m + \Gamma_m}. \tag{S10}$$

As an example, we calculate and plot in Fig. S4a the off-diagonal polarizability of a composite with a gold nanoparticle of 5 nm radius. The TLS is 8 nm apart from the nanoparticle along the x-axis. The bandwidth is significantly broadened by the gold nanoparticle and the enhancement can be up to 38. The spectrum is shifted about $36\gamma_0$. For such a composite, the effective dipole moment of the TLS is enlarged by the gold nanoparticle and it can be estimated by the curves in Fig. S4a by ultizing Eq. (S10).

Here we have neglected the magneitzation of the plasmon in the metal nanoparticle because its contribution is orders of magntidue smaller. The permittivity of the metal under an external magnetic field in the z direction can be expressed by a tensor as [10]

$$\overleftrightarrow{\boldsymbol{\varepsilon}}(\omega) = 1 - \frac{\omega_{\mathrm{p}}^2}{\left(\omega + \frac{i}{\tau}\right)^2 - \omega_B^2} \times \begin{pmatrix} 1 + \frac{i}{\tau\omega} & \frac{i\omega_B}{\omega} & 0 \\ -\frac{i\omega_B}{\omega} & 1 + \frac{i}{\tau\omega} & 0 \\ 0 & 0 & \frac{\left(\omega + \frac{i}{\tau}\right)^2 - \omega_B^2}{\omega\left(\omega + \frac{i}{\tau}\right)} \end{pmatrix}, \tag{S11}$$

where ω_{p} is the plasmon frequency and τ is the decay time caused by metal loss. $\omega_B = eB/m$ is the cyclotron frequency with e and m denoting the charge and mass of an electron, respectively. Under $B = 0.56\mathrm{T}$, the off-diagonal element is equal to 6×10^{-6}, which is 5 orders less than diagonal elements. Thus we can neglect the effect from the magnetic field in the metal materials.

B. Deviration of Eqs. (2) and (3) from self-consistent form

We apply a *self-consistent* approach, which includes all the interactions. It is consistent with spirit of coupled dipole approximation (CDA). Here, we show the derivation of Eq. (2), which can be also found in Ref. [14].

The total field can be written as the addition of three field:

$$\mathbf{E}(\mathbf{r}) = \mathbf{E}_0(\mathbf{r}) + \mathbf{E}_0^s(\mathbf{r}) + \overleftrightarrow{\mathbf{G}}(\mathbf{r}, \mathbf{r}_{\mathrm{TLS}}, \omega) \cdot \overleftrightarrow{\mathbf{V}} \cdot \mathbf{E}(\mathbf{r}_{\mathrm{TLS}}), \tag{S12}$$

where $\mathbf{E}_0(\mathbf{r}) + \mathbf{E}_0^s(\mathbf{r})$ is the field in the absence of the TLS, which can be calculated from the Mie scattering theory. The last term describes the modification of the field introduced by TLS. It is important to note that the response of the nanoparticle due to excitation of TLS is also included because the dyadic Green's function $\overleftrightarrow{\mathbf{G}}(\mathbf{r}, \mathbf{r}')$ includes the nanoparticle. The dyadic Green's function can be decomposed as $\overleftrightarrow{\mathbf{G}}(\mathbf{r}, \mathbf{r}') = \overleftrightarrow{\mathbf{G}}_0(\mathbf{r}, \mathbf{r}') + \overleftrightarrow{\mathbf{G}}_{\mathrm{s}}(\mathbf{r}, \mathbf{r}')$, where $\overleftrightarrow{\mathbf{G}}_0(\mathbf{r}, \mathbf{r}')$ is the Green's function in free space and $\overleftrightarrow{\mathbf{G}}_s(\mathbf{r}, \mathbf{r}')$ is the scattered Green's function. $\overleftrightarrow{\mathbf{V}} = V(\omega)\boldsymbol{\mu} \cdot \boldsymbol{\mu}^\dagger = \left(\frac{\omega^2}{\hbar c^2 \varepsilon_0} \frac{1}{\omega - \omega_0}\right) \boldsymbol{\mu} \cdot \boldsymbol{\mu}^\dagger$ is the optical potential. The above equation is *self-consistent* in that the field $\mathbf{E}(\mathbf{r})$ is unknown and shows up on both side of the equation. Eq. (S12) can also be written in an iterative form as

$$\begin{aligned} \mathbf{E}(\mathbf{r}) = {} & [\mathbf{E}_0(\mathbf{r}) + \mathbf{E}_0^{\mathrm{s}}(\mathbf{r})] + \overleftrightarrow{\mathbf{G}}(\mathbf{r}, \mathbf{r}_{\mathrm{TLS}}) \cdot \overleftrightarrow{\mathbf{V}} \cdot [\mathbf{E}_0(\mathbf{r}) + \mathbf{E}_0^{\mathrm{s}}(\mathbf{r})] \\ & + \overleftrightarrow{\mathbf{G}}(\mathbf{r}, \mathbf{r}_{\mathrm{TLS}}, \omega) \cdot \overleftrightarrow{\mathbf{V}} \cdot \overleftrightarrow{\mathbf{G}}(\mathbf{r}, \mathbf{r}_{\mathrm{TLS}}, \omega) \cdot \overleftrightarrow{\mathbf{V}} \cdot [\mathbf{E}_0(r) + \mathbf{E}_0^{\mathrm{s}}(\mathbf{r})] + \cdots \end{aligned} \tag{S13}$$

The infinite series can be summed to give

$$\mathbf{E}(\mathbf{r}) = \mathbf{E}_0(\mathbf{r}) + \mathbf{E}_0^{\mathrm{s}}(\mathbf{r}) + \overleftrightarrow{\mathbf{G}}(\mathbf{r}, \mathbf{r}_{\mathrm{TLS}}, \omega) \cdot \overleftrightarrow{\mathbf{T}} \cdot [\mathbf{E}_0(\mathbf{r}) + \mathbf{E}_0^{s}(\mathbf{r})], \tag{S14}$$

where the single TLS T-matrix is given by $\overleftrightarrow{\mathbf{T}} = \left[\frac{V(\omega)}{1-V(\omega)\boldsymbol{\mu}_0^{\dagger}\cdot\overleftrightarrow{\mathbf{K}}(\mathbf{r},\mathbf{r}_{\mathrm{TLS}},\omega)\cdot\boldsymbol{\mu}_0}\right]\boldsymbol{\mu}_0 \cdot \boldsymbol{\mu}_0^{\dagger}$ and $\overleftrightarrow{\mathbf{K}}(\mathbf{r}, \mathbf{r}_{\mathrm{TLS}}, \omega) = \overleftrightarrow{\mathbf{G}}(\mathbf{r}, \mathbf{r}_0, \omega) - \frac{c^2}{\varepsilon_0 \omega^2}\delta(\mathbf{r} - \mathbf{r}_0)\overleftrightarrow{\mathbf{I}}$. After substituting the optical potential into Eq. (S14), the total field is written as

$$\mathbf{E}(\mathbf{r}) = \mathbf{E}_0(\mathbf{r}) + \mathbf{E}_0^{\mathrm{s}}(\mathbf{r}) + \frac{\omega^2}{\hbar\varepsilon_0 c^2}\overleftrightarrow{\mathbf{G}}(\mathbf{r}, \mathbf{r}_{\mathrm{TLS}}, \omega) \cdot \left[\frac{\boldsymbol{\mu}_0^{\dagger} \cdot \left(\mathbf{E}_0(\mathbf{r}) + \mathbf{E}_0^{\mathrm{s}}(\mathbf{r})\right)}{\omega - \omega_0 + \frac{\omega^2}{\hbar\varepsilon_0 c^2}\boldsymbol{\mu}_0^{\dagger} \cdot \overleftrightarrow{\mathbf{K}}(\mathbf{r}, \mathbf{r}_{\mathrm{TLS}}, \omega) \cdot \boldsymbol{\mu}_0}\right]\boldsymbol{\mu}_0. \tag{S15}$$

Lamb shift + the modified decay rate is written as $\delta\omega_0 + i\Gamma/2 = \frac{\omega^2}{\hbar\varepsilon_0 c^2}\boldsymbol{\mu}^{\dagger} \cdot \overleftrightarrow{\mathbf{K}}(\mathbf{r}, \mathbf{r}_{\mathrm{TLS}}, \omega) \cdot \boldsymbol{\mu}$. Then the total field is given by

$$\mathbf{E}(\mathbf{r}) = \mathbf{E}_b(\mathbf{r}) + \frac{\omega^2}{\varepsilon_0 c^2}\overleftrightarrow{\mathbf{G}}(\mathbf{r}, \mathbf{r}_{\mathrm{TLS}}, \omega) \cdot \mathbf{d}, \tag{S16}$$

where the induced dipole moment is $\mathbf{d} = \frac{1}{\hbar}\frac{\boldsymbol{\mu}_0^{\dagger}\cdot[\mathbf{E}_0(\mathbf{r}_{\mathrm{TLS}})+\mathbf{E}_0^{s}(\mathbf{r}_{\mathrm{TLS}})]}{\omega-\omega_0+\delta\omega_0+i\Gamma/2}\boldsymbol{\mu}_0$ and the background field is $\mathbf{E}_{\mathrm{b}}(\mathbf{r}) = \mathbf{E}_0(\mathbf{r}) + \mathbf{E}_0^{\mathrm{s}}(\mathbf{r})$.

C. Polarizability of a magnetized TLS , and a magnetized TLS-nanoparticle composite

Here, in this section, we calculate the polarizability of quantum-classical composites. First, for a bare single TLS under a magnetic field, the induced dipole moment (polarizability) is given by

$$\mathbf{d}_{\mathrm{TLS}}^{(0)}(\omega) = \frac{1}{\hbar}\sum_m \frac{\boldsymbol{\mu}_m^{\dagger} \cdot \mathbf{E}_0(\mathbf{r}_{\mathrm{TLS}})}{\delta_m + i\gamma_m/2}\boldsymbol{\mu}_m = \overleftrightarrow{\boldsymbol{\alpha}}_{\mathrm{TLS}}^{(0)}(\omega) \cdot \mathbf{E}_0(\mathbf{r}_{\mathrm{TLS}}), \tag{S17}$$

where the detuning is $\delta_m = \omega - \omega_m$ and $m = \pm,0$ respectively denote the $\sigma^{\pm}, \sigma^z$ transition dipole moments with $\boldsymbol{\mu}_{\pm} = \frac{\mu_0}{\sqrt{2}}(1, \pm i, 0)^{\mathrm{T}}$ and $\boldsymbol{\mu}_0 = \mu_0(0, 0, 1)^{\mathrm{T}}$. The polarizability tensor of a bare TLS is written as

$$\overleftrightarrow{\boldsymbol{\alpha}}_{\mathrm{TLS}}^{(0)}(\omega)=\begin{pmatrix}\alpha_{xx} & \alpha_{xy} & 0\\ \alpha_{yx} & \alpha_{yy} & 0\\ 0 & 0 & \alpha_{zz}\end{pmatrix}. \tag{S18}$$

We can calculate the induced dipole moment for three orthogonal electric fields $\mathbf{E}_0=(E_0,0,0)^T$, $(0,E_0,0)^T$, and $(0,0,E_0)^T$. We obtain three results:

$$\mathbf{d}_{\mathrm{TLS}}^{(0)}(\omega)=\frac{E_0}{\sqrt{2}}\left(\alpha_{xx},\alpha_{yx},0\right)^T=\frac{\mu_0^2E_0}{\hbar}\left(\frac{1}{2\delta_+ +i\gamma_+}+\frac{1}{2\delta_- +i\gamma_-},\frac{i}{2\delta_+ +i\gamma_+}-\frac{i}{2\delta_- +i\gamma_-},0\right)^T,$$

$$\mathbf{d}_{\mathrm{TLS}}^{(0)}(\omega)=\frac{E_0}{\sqrt{2}}\left(\alpha_{xy},\alpha_{yy},0\right)^T=\frac{\mu_0^2E_0}{\hbar}\left(\frac{-i}{2\delta_+ +i\gamma_+}+\frac{i}{2\delta_- +i\gamma_-},\frac{1}{2\delta_+ +i\gamma_+}+\frac{1}{2\delta_- +i\gamma_-},0\right)^T,$$

$$\mathbf{d}_{\mathrm{TLS}}^{(0)}(\omega)=E_0(0,0,\alpha_{zz})^T=\frac{2\mu_0^2E_0}{\hbar}\left(0,0,\frac{1}{2\delta_0+i\gamma_0}\right)^T. \tag{S19}$$

By combining the above results and assuming same radiative bandwidths for both transitions ($\gamma_\pm=\gamma_0$ and γ_0 is the natural linewidth of TLS), we obtain the explicit form of the polarizability tensor

$$\overleftrightarrow{\boldsymbol{\alpha}}_{\mathrm{TLS}}^{(0)}(\omega)=\frac{\mu_0^2}{\hbar}\begin{pmatrix}\frac{\sqrt{2}}{2\delta_+ +i\gamma_0}+\frac{\sqrt{2}}{2\delta_- +i\gamma_0} & -\frac{\sqrt{2}i}{2\delta_+ +i\gamma_0}+\frac{\sqrt{2}i}{2\delta_- +i\gamma_0} & 0\\ \frac{\sqrt{2}i}{2\delta_+ +i\gamma_0}-\frac{\sqrt{2}i}{2\delta_- +i\gamma_0} & \frac{\sqrt{2}}{2\delta_+ +i\gamma_0}+\frac{\sqrt{2}}{2\delta_- +i\gamma_0} & 0\\ 0 & 0 & \frac{2}{2\delta_0+i\gamma_0}\end{pmatrix}, \tag{S20}$$

where $\delta_\pm=\omega-\omega_0\pm\delta\omega_{\mathrm{B}}$. The Zeeman splitting energy is given by $\delta\omega_B=\frac{g\mu_B}{\hbar}B$ and the g-factor is determined by the details of a TLS. When the incident frequency is at σ^+ transition frequency, the detuning $\delta_+=0$. Considering that $\delta_-\gg\gamma_0$, we have

$$\overleftrightarrow{\boldsymbol{\alpha}}_{\mathrm{TLS}}^{(0)}(\omega=\omega_\pm)\approx\frac{\alpha_0}{\sqrt{2}}\begin{pmatrix}1 & \pm i & 0\\ \mp i & 1 & 0\\ 0 & 0 & 0\end{pmatrix}, \tag{S21}$$

where $\alpha_0=i\frac{3}{4\pi^2}\varepsilon_b\varepsilon_0\lambda_a^3$ is the resonant polarizability of the TLS in free space. Here we have assumed the Zeeman splitting is greater than the natural linewidth, i.e. $|\omega_+-\omega_-|>\gamma_0$.

TLS-nanoparticle composite--For the case of a TLS near a nanoparticle, the total induced dipole moment is given by

$$\mathbf{d}(\omega) = \mathbf{d}_{\mathrm{TLS}}(\omega) + \mathbf{p}_{\mathrm{NP}}(\omega) = \overleftrightarrow{\boldsymbol{\alpha}}^{(\mathrm{eff})}(\omega) \cdot \mathbf{E}_0, \tag{S22}$$

where

$$\mathbf{d}_{\mathrm{TLS}}(\omega) = \frac{1}{\hbar}\sum_m \frac{\boldsymbol{\mu}_m^{\dagger}\cdot[\mathbf{E}_0(\mathbf{r}_{\mathrm{TLS}})+\mathbf{E}_0^{\mathrm{s}}(\mathbf{r}_{\mathrm{TLS}})]}{\Delta_m + i\Gamma_m/2}\boldsymbol{\mu}_m = \overleftrightarrow{\boldsymbol{\alpha}}_{\mathrm{TLS}}^{(\mathrm{eff})}(\omega) \cdot \mathbf{E}_0, \tag{S23}$$

$$\mathbf{p}_{\mathrm{NP}}(\omega) = \varepsilon_0(\varepsilon_{\mathrm{NP}} - \varepsilon_{\mathrm{b}})\int d^3r\mathbf{E}(\mathbf{r},\omega) \approx 3V\varepsilon_0 \frac{\tilde{\varepsilon}_{\mathrm{NP}} - \varepsilon_{\mathrm{b}}}{\tilde{\varepsilon}_{\mathrm{NP}} + 2\varepsilon_{\mathrm{b}}}[\mathbf{E}_0(\mathbf{r}_{\mathrm{NP}}) + \mathbf{E}_{\mathrm{TLS}}^{s}(\mathbf{r}_{\mathrm{NP}})], \tag{S24}$$

where $\mathbf{E}_{\mathrm{TLS}}^{\mathrm{s}}(\mathbf{r}) = \frac{\omega^2}{\varepsilon_0 c^2}\overleftrightarrow{\mathbf{G}}(\mathbf{r},\mathbf{r}_{\mathrm{TLS}},\omega)\cdot\mathbf{d}_{\mathrm{TLS}}$ is the scattering field of the TLS. Dielectric constants of vacuum, background and nanoparticle are denoted by $\varepsilon_{0,\mathrm{b,NP}}$, respectively. Thus, the system described by Eqs. (S23) and (S24) is self-consistent. Here, the decay rate of TLS Γ_m is modified by the nanoparticle and it is calculated from Eq. (S8). If the size of the TLS-nanoparticle composite system is in deep subwavelength scale, the total polarizability tensor is given by

$$\overleftrightarrow{\boldsymbol{\alpha}}^{(\mathrm{eff})}(\omega) = \overleftrightarrow{\boldsymbol{\alpha}}_{\mathrm{TLS}}^{(\mathrm{eff})}(\omega) + \overleftrightarrow{\boldsymbol{\alpha}}_{\mathrm{NP}}^{(\mathrm{eff})}(\omega). \tag{S25}$$

If assuming the TLS-nanoparticle related location is same to Fig. 3a, the effective polarizability tensor of the TLS is

$$\overleftrightarrow{\boldsymbol{\alpha}}_{\mathrm{TLS}}^{(\mathrm{eff})}(\omega) = \frac{E_0 + E_0^s}{E_0}\frac{\mu_0^2}{\hbar}\begin{pmatrix} \frac{\sqrt{2}}{2\Delta_+ + i\Gamma_+} + \frac{\sqrt{2}}{2\Delta_- + i\Gamma_-} & -\frac{\sqrt{2}i}{2\Delta_+ + i\Gamma_+} + \frac{\sqrt{2}i}{2\Delta_- + i\Gamma_-} & 0 \\ \frac{\sqrt{2}i}{2\Delta_+ + i\Gamma_+} - \frac{\sqrt{2}i}{2\Delta_- + i\Gamma_-} & \frac{\sqrt{2}}{2\Delta_+ + i\Gamma_+} + \frac{\sqrt{2}}{2\Delta_- + i\Gamma_-} & 0 \\ 0 & 0 & \frac{2}{2\Delta_0 + i\Gamma_0} \end{pmatrix}, \tag{S26}$$

where $\Gamma_{\pm,0}$ are obtained from Eq. (S8). The superscript "(eff)" denotes the polarizability is an effective quantity that has been dressed by TLS. Note that the detuning and decay rates are modified by the nearby nanoparticle and thus we use Δ and Γ to represent them. By similar derivation as before, the effective polarizability tensor without radiative correction is given by

$$\overleftrightarrow{\boldsymbol{\alpha}}_{\mathrm{NP}}^{(\mathrm{eff})}(\omega) = 3V\varepsilon_0 \frac{\tilde{\varepsilon}_{\mathrm{NP}} - \varepsilon_{\mathrm{b}}}{\tilde{\varepsilon}_{\mathrm{NP}} + 2\varepsilon_{\mathrm{b}}} \left[\overleftrightarrow{\mathbf{I}} + \frac{\omega^2}{\varepsilon_0 c^2} \overleftrightarrow{\mathbf{G}}_0(\mathbf{r}_{\mathrm{NP}}, \mathbf{r}_{\mathrm{TLS}}, \omega) \cdot \overleftrightarrow{\boldsymbol{\alpha}}_{\mathrm{TLS}}^{(\mathrm{eff})}(\omega) \right]. \tag{S27}$$

If the gold permittivity with loss is applied, the induced dipole moment of the nanoparticle $\mathbf{p}_{\mathrm{NP}}$ is much smaller than $\mathbf{d}_{\mathrm{TLS}}$.

In Fig. S4, we plot the off-diagonal element of polarizability tensor α_{xy} in Eq. (S22) as a function of frequency with a fixed distance between the TLS and nanoparticle. Right figure shows the bandwidth enhancement and maximum $|\alpha_{xy}|$ as variation of TLS-nanoparticle distance.

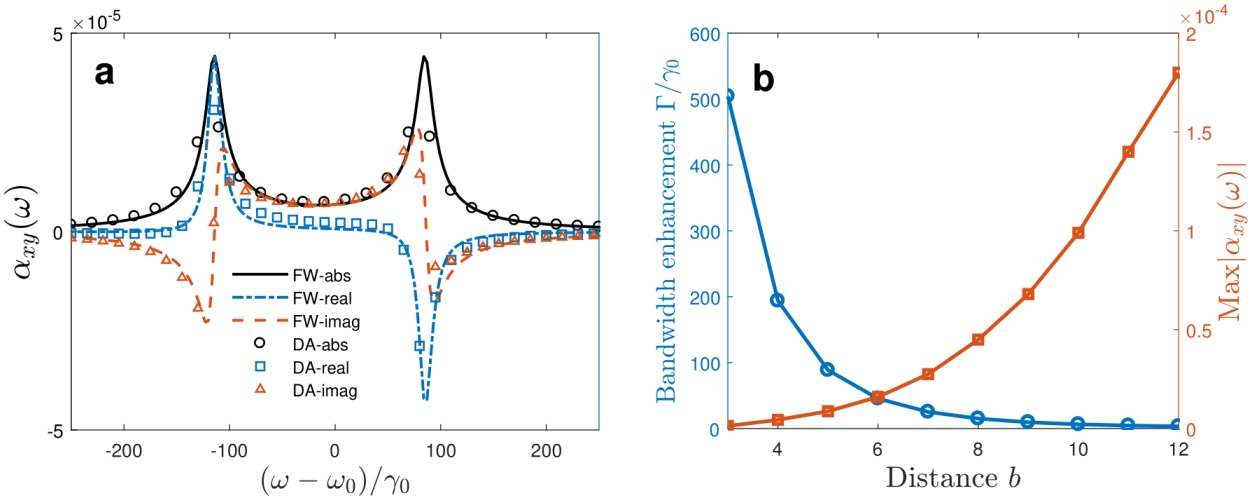

FIG. S4 (a) The off-diagnal polarizability α_{xy} of a composite versus frequency. The comosite contains a magnetized TLS which is 8 nm away from the surface of the gold nanoparticle of 5 nm along z axis. The background dielectric constant is $\varepsilon_{\mathrm{b}} = 2.25$ and and the Zeeman splitting $\delta\omega_{\mathrm{B}} = 200\gamma_0$. Curves are calculated from Eq. (S9,S10) and circles are from the dipole approximation (DA) for the nanoparticle. (b) Bandwidth enhancement Γ/γ_0 and maximum value of off-diagonal polarizability as a function of the TLS-nanoparticle distance b.

D. Degree of Circular Polarization of a TLS-nanoparicle composite

For a bare TLS, Eq. (S21) already indicates that only circular polarizations are induced at frequency of transition $\sigma^{\pm}$. A quantity, called degree of circular polarization (DOCP), describes the ratio of circular polarization in a small unit. Its definition is given by [20]

$$\mathbf{DOCP} = -i \frac{d_x d_y^* - d_y d_x^*}{d_x d_x^* + d_y d_y^*}, \tag{S28}$$

where $d_x = (1/\sqrt{2})(d_+ + d_-)$ and $d_y = (-i/\sqrt{2})(d_+ - d_-)$. $d_\pm$ are the induced dipole moments of transitions $\sigma^\pm$. For a TLS-nanoparticle composite in Fig. 4a, we plot the DOCP as a function of frequency in Fig. S5 and its peak and valley values are close to $\pm$100%, which denote pure CW and CCW polarizations, respectively.

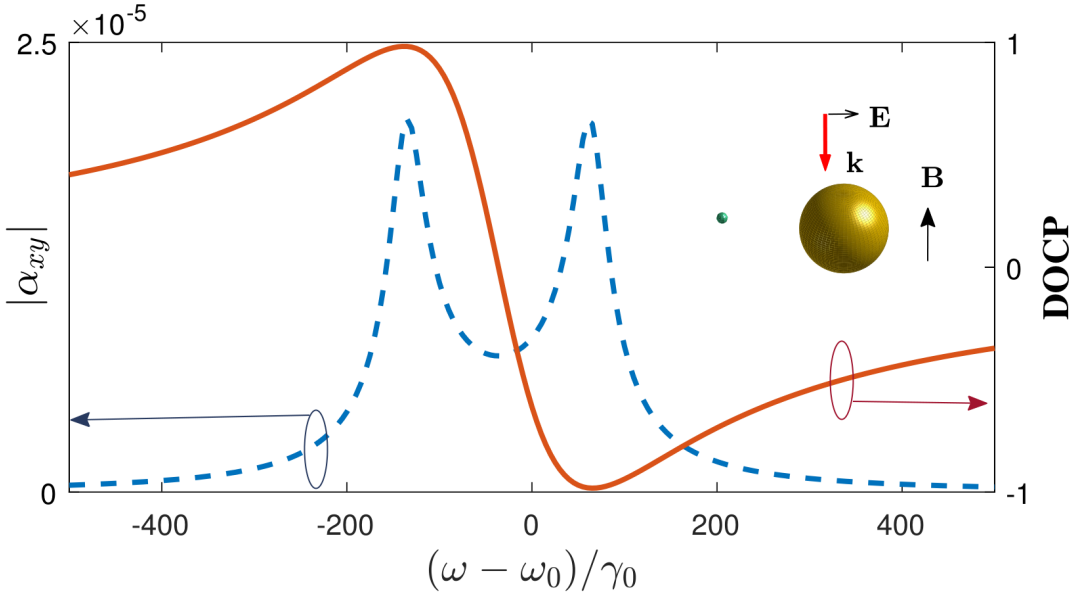

FIG. S5 Off-diagonal element of polarizability tensor (blue) and DOCP (red) as a function of frequency. The composite setting is same to Fig. 4a in main text.

E. A TLS with large nonradiative decay rate interacting with a nanoparticle

The scattering cross section of a TLS is determined by the radiative (γ_{rad}) and non-radiative (γ_{non}) decay rates as

$$\sigma(\omega) = \frac{3\lambda^2}{2\pi} \frac{\gamma_{\mathrm{rad}}^2}{4(\omega-\omega_0)^2 + (\gamma_{\mathrm{rad}}+\gamma_{\mathrm{non}})^2}, \tag{S29}$$

where ω_0 is the TLS transition frequency and λ is the wavelength. The maximum value of the scattering cross section is given by $\sigma_{max} = \frac{3\lambda^2}{2\pi} \frac{\gamma_{\mathrm{rad}}^2}{(\gamma_{\mathrm{rad}}+\gamma_{\mathrm{non}})^2}$ and we plot σ_{max} as a function of $\gamma_{\mathrm{non}}/\gamma_{\mathrm{rad}}$ in Fig. S6a.

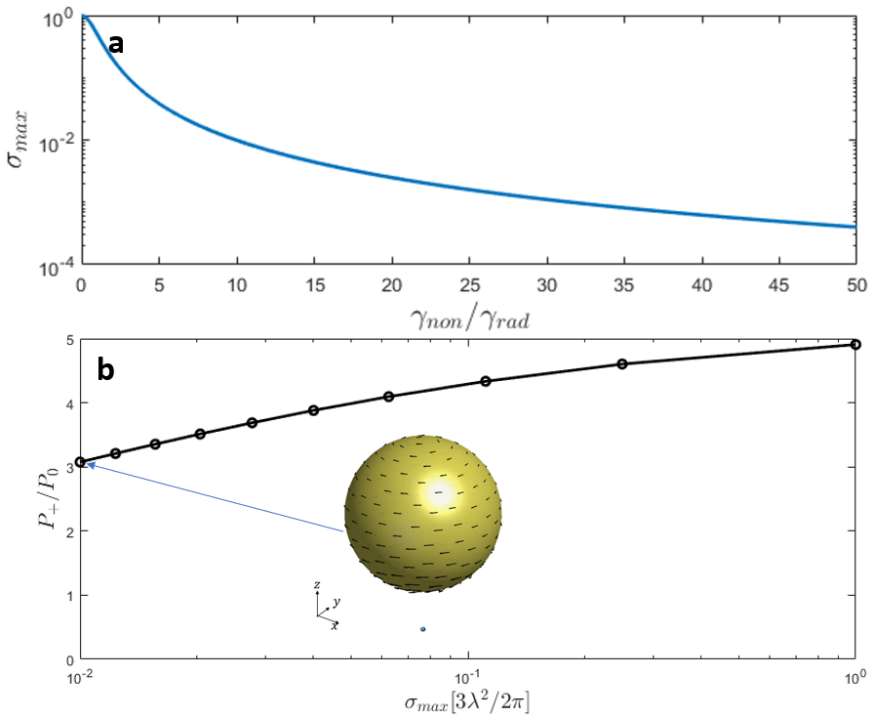

FIG. S6. (a) The maximum value of the scattering cross section as a function of the ratio between non-radiative and radiative decay rates. (b) The circular polarization as a function of maximum scattering cross section. (Inset) The circular polarization of the gold nanoparticle as shown its surface currents at $\sigma_{max} = 0.01 \times 3\lambda^2/2\pi$. The TLS-nanoparticle distance is b = 8nm and nanoparticle radius is a = 5nm.

Atoms have decoherence that effectively increases the ratio when embedded, leading to small cross section. For some specific quantum dots, the ratio is small due to the large dipole size and weak phonon exciton coupling. For example, $\gamma_{\mathrm{non}}/\gamma_{\mathrm{rad}}$~0.1 in Ref. [15,16] and even $\gamma_{\mathrm{non}}/\gamma_{\mathrm{rad}}$~0.01 in Ref. [17].

Even when the cross section is well below the ideal maximum $3\lambda^2/2\pi$, we still obtain similar effect as shown in Fig. 3a&b. For example, at a small cross section ($0.01 \times 3\lambda^2/2\pi$), the clockwise circular dipole moment of the nanoparticle is $3P_0$, where $P_0 = |\alpha_{NP}|E_0$ is the dipole moment induced by background field. The induced dipole moment of the nanoparticle is given by $\mathbf{P} = \varepsilon_0(\varepsilon_{NP} - \varepsilon_b) \iiint \mathbf{E}(\mathbf{r}) d^3r$, where $\mathbf{E}(\mathbf{r})$ is the total field. P_+ is the induced dipole moment of transition σ^+, which is obtained from $\mathbf{P}$. Its relation to the maximum cross section is shown in Fig. S4b.

F. A cluster of composite systems with dipole approximation

Next, we consider a cluster of quantum-classical composite systems. For a cluster of quantum-classcial composite, it's very computational-intensive to solve the exact optical Bloch equations. However, as the size of the nanoparticle is much smaller than the wavelength, nanoparticles can be treated as dipoles. The dipole moment of a small nanoparticle located at position **r** is written as

$$\mathbf{P}(\mathbf{r}) = \varepsilon_0 \varepsilon_b \alpha \mathbf{E}_0(\mathbf{r}), \tag{S30}$$

where the polarizability of a small sphere with radiative correction is given by [11,12]

$$\alpha = \frac{\alpha_0}{1 - i(\mathrm{k}^3/6\pi\varepsilon_0)\alpha_0}, \tag{S31}$$

$$\alpha_0 = 4\varepsilon_0 \varepsilon_b \pi a^3 \frac{\tilde{\varepsilon}_{\mathrm{NP}} - \varepsilon_{\mathrm{b}}}{\tilde{\varepsilon}_{\mathrm{NP}} + 2\varepsilon_{\mathrm{b}}}.$$

The nonlocal permittivity of the nanoparticle is corrected as [18,19] $\tilde{\varepsilon}_{\mathrm{NP}} = \varepsilon_{\mathrm{NP}}/(1 + \delta_{\mathrm{NL}})$, where $\delta_{\mathrm{NL}} = \frac{\varepsilon_{\mathrm{NP}} - \varepsilon_\infty}{\varepsilon_\infty} \frac{j_1(k_{\mathrm{NL}}a)}{k_{\mathrm{NL}} a j_1'(k_{\mathrm{NL}}a)}$ and the Drude permittivity is $\varepsilon_{\mathrm{NP}} = \varepsilon_\infty - \frac{\omega_p^2}{\omega^2 + i\gamma\omega}$. $k_{\mathrm{NL}} = \sqrt{\frac{\omega^2 + i\omega\gamma - \omega_{\mathrm{p}}^2}{\beta^2 + D\gamma - iD\omega}}$ is the wave vector of the longitudinal wave. The parameters are $\varepsilon_\infty = 9.84, \omega_{\mathrm{p}} = 9.01eV, \gamma = 0.072eV, \sqrt{\mathrm{D}/\omega_{\mathrm{p}}} = 1.3\mathrm{nm}, v_{\mathrm{F}}/\omega_{\mathrm{p}} = 0.11\mathrm{nm}$.

The scattering field then is calculated as

$$\mathbf{E}_{\mathrm{s}}(\mathrm{r}) = \frac{\omega^2}{c^2 \varepsilon_0} \overleftrightarrow{\mathbf{G}}_0(\mathrm{r}, \mathrm{r}'; \omega) \cdot \mathbf{P}(\mathrm{r}') \tag{S32}$$

and

$$\begin{aligned} \overleftrightarrow{\mathbf{G}}_0(\mathbf{r}, \mathbf{r}'; \omega) = \frac{e^{-i\omega/c\Delta r}}{4\pi\varepsilon_0 R^3} [&(\frac{\omega^2 \Delta r^2}{c^2} - i\frac{\omega \Delta r}{c} - 1)\overleftrightarrow{\mathbf{I}} \\ &-(\frac{\omega^2 \Delta r^2}{c^2} - 3i\frac{\omega \Delta r}{c} - 3)\Delta\mathbf{r} \cdot \Delta\mathbf{r}^{\dagger}] \end{aligned} \tag{S33}$$

is the free-space dyadic Green's function, where $\Delta\mathbf{r} = \mathbf{r} - \mathbf{r}'$, $\Delta r = |\Delta\mathbf{r}|$ and $\overleftrightarrow{\mathbf{I}}$ is the identity matrix.

For a cluster of composite systems, we modify the sub- and super-scripts and use subscripts "i, j" denote the TLSs and subscripts "I, J" denote the nanoparticles. The superscripts "m, n" represent polarization indexes for TLSs and nanoparticles. The induced dipole moments are given by

$$\mathbf{d}_i^n = \langle \hat{S}_i^n \rangle \boldsymbol{\mu}_i^n = \frac{2\boldsymbol{\mu}_i^n \cdot \left[\mathbf{E}_0(\mathbf{r}_i) + \sum_{j\neq i,m} \langle \mathbf{E}_j^m(\mathbf{r}_i)\rangle + \sum_{J\neq I,m} \mathbf{E}_J^m(\mathbf{r}_I)\right]}{\hbar\left(\delta_i^m + \frac{i\gamma_0}{2}\right)} \boldsymbol{\mu}_i^n \qquad \text{for TLSs,}$$

$$\mathbf{p}_I^n = \boldsymbol{\nu}_I^n p_I^n = 4\varepsilon_0\varepsilon_b \pi a^3 \frac{\tilde{\varepsilon}_{NP} - \varepsilon_b}{\tilde{\varepsilon}_{NP} + 2\varepsilon_b} \times \tag{S34}$$

$$\boldsymbol{\nu}_I^n \cdot \left[\mathbf{E}_0(\mathbf{r}_I) + \sum_{j,m} \langle \mathbf{E}_j^m(\mathbf{r}_I)\rangle + \sum_{J\neq I,m} \mathbf{E}_J^m(\mathbf{r}_I)\right] \qquad \text{for NPs,}$$

where $\mathbf{E}_{m,M}^s(\mathbf{r})$ is the field at position $\mathbf{r}$ scattered from mth TLS or Mth nanoparticle and they are determined by their induced dipole moments. $\boldsymbol{\nu}_I^n$ is a unit vector along $n = x, y, z$ axis. This self-consistent problem can be written in a seriers of nonhomogeneous linear equations:

$$\begin{aligned}
&\hbar(\Delta_i^n + i\gamma_0/2)\langle \hat{S}_i^n \rangle + \frac{\omega^2}{c^2\varepsilon_0} \boldsymbol{\mu}_i^{n\dagger} \cdot \sum_{j\neq i,m} \overleftrightarrow{\mathbf{G}}_0(\mathbf{r}_i, \mathbf{r}_j) \cdot \boldsymbol{\mu}_j^m \langle \hat{S}_j^m \rangle \\
&+ \frac{\omega^2\mu_0}{c^2\varepsilon_0} \boldsymbol{\mu}_i^{n\dagger} \cdot \sum_{J,m} \overleftrightarrow{\mathbf{G}}_0(\mathbf{r}_i, \mathbf{r}_J) \cdot \boldsymbol{\nu}_J^m p_J^m = -\boldsymbol{\mu}_i^{n\dagger} \cdot \mathbf{E}_0(\mathbf{r}_i), \\
&-\frac{\mu_0}{A} p_I^n + \frac{\omega^2\mu_0}{c^2\varepsilon_0} \boldsymbol{\nu}_I^n \cdot \sum_{J\neq I,m} \overleftrightarrow{\mathbf{G}}_0(\mathbf{r}_I, \mathbf{r}_J) \cdot \boldsymbol{\nu}_J^m p_J^m \\
&+ \frac{\omega^2}{c^2\varepsilon_0} \boldsymbol{\nu}_I^{n\dagger} \cdot \sum_{j,m} \overleftrightarrow{\mathbf{G}}_0(\mathbf{r}_I, \mathbf{r}_j) \cdot \boldsymbol{\mu}_j^m \langle \hat{S}_j^m \rangle = -\boldsymbol{\nu}_I^{n\dagger} \cdot \mathbf{E}_0(\mathbf{r}_I).
\end{aligned} \tag{S35}$$

The total field of the composite is then given by

$$\langle \mathbf{E}_{\text{tot}}(\mathbf{r}, \omega)\rangle = \mathbf{E}_0(\mathbf{r}) + \frac{\omega^2}{c^2\varepsilon_0}\left[\sum_{i,n} \overleftrightarrow{\mathbf{G}}_0(\mathbf{r}, \mathbf{r}_i; \omega) \cdot \boldsymbol{\mu}_i^n \langle \hat{S}_i^n \rangle + \sum_{I,n} \overleftrightarrow{\mathbf{G}}_0(\mathbf{r}, \mathbf{r}_I; \omega) \cdot \boldsymbol{\nu}_I^n p_I^n\right]. \tag{S36}$$

The accuracy of the dipole approximation can be verified by comparing the results obtained from exact calculation (curves) and dipole approximation (markers) in Fig. S4a. The results obtained

from both appraoches match well. In our calculations, we use the nonlocal permittivity $\tilde{\varepsilon}_{\mathrm{NP}}$ with Landau damping and the polarizability with radiative correction.

IV. Single composite with multiply TLSs

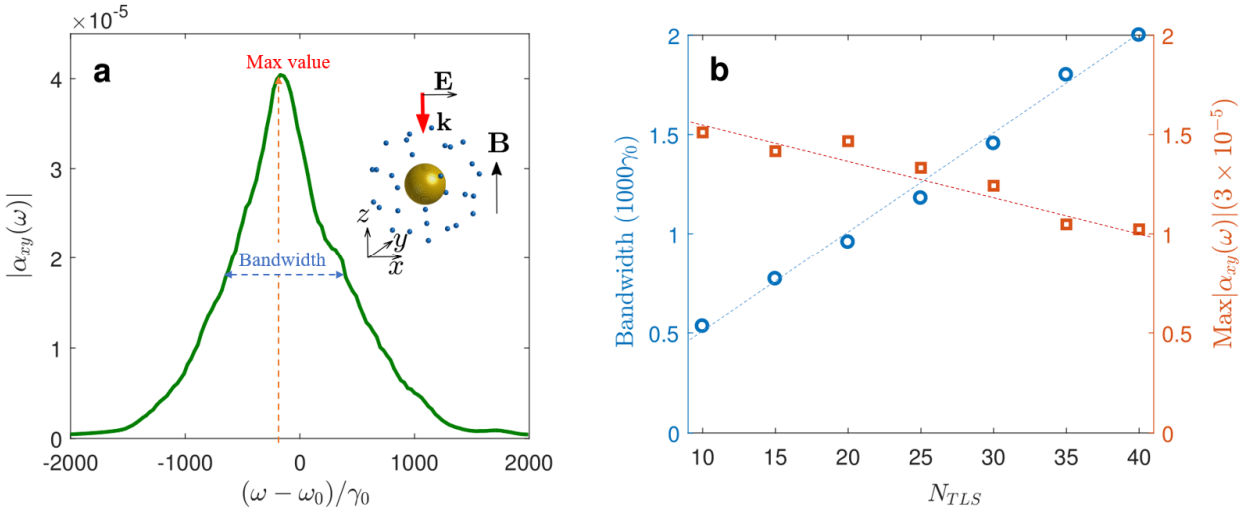

FIG. S7 (a) Average off-diagonal prolarizability of a composite with multiply TLSs ($N_{\mathrm{TLS}} = 25$) with frequency banwidth $\Delta\omega = 1250\gamma_0$ and single gold nanoparticles on as a function of frequency. a and b are same in Fig. S5. (a) and the Zeeman splitting is $\Delta\omega_B = 200\gamma_0$. (b) The bandwidth (blue circles) and maximum value of off-diagnal polarizability (red squares), defined in (a), as a function of TLS number. Dashed lines are the linear fittings.

In a single composite, the bandwidth can be further broadened by adding more TLSs. As an example, we consider 25 TLSs that are randomly distributed around a nanoparticle (inset in Fig. S7a) and calcualte the average off-diagonal probability. As shown by the spectrum in Fig. S7a, the bandwidth is broadened to $1200\gamma_0$. The correspoinding bandwidth and maximum off-diagonal polarizability are obtained and plotted in Fig. S7b. Both the bandwidth (blue circles) and the maximum off-diagonal polarizability (red squares) are approximately linear with respect to the number of TLSs.

V. Quantum-classical materials

In this section, we discuss the modeling of the embeding large number of magnetized TLS-nanoparticle composites in a hosting material. The the simulation of this composite material is

based on the Sec. IV C. The induced dipole moments of all TLSs and nanoparticles can be solved frome the non-homogeneous Eqs. (S35), which are expressed into a matrix equation in simulation. This matrix equation is the kernal of the simulation. The electric field can be calculated based on Eq. (S36).

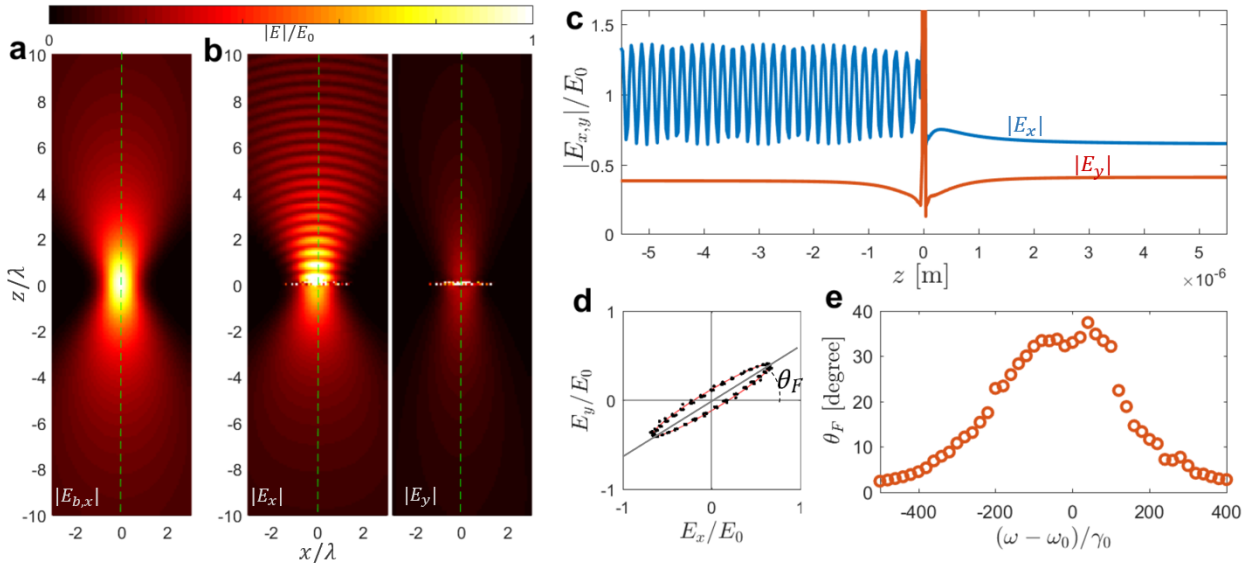

FIG. S8 (a) Spatial distribution of the absolute value of incident Gaussian beam at frequency $\omega = \omega_0 - 20\gamma_0$. (b) Spatial distributions of the absolute values of the x and y components of the total electric field. (c) Electric fields along green lines in (b) for quantum calculations. (d) Polarization of outgoing field. (e) The Faraday rotation angle as a function of frequency for single sample of the composite material.

We consider a disk with a radius of 550 nm and height of 45 nm, filled with about 300 composites randomly distributed. In each composite, 10 TLSs are randomly surrounding a gold nanoparticle with radius 5 nm and spacing 8 nm. This is a computationally expensive simulation, considering that we model the response of each TLS and nanoparticle without using any effective medium assumption. For example, such a composite material, the matrix size in simulation can be larger than 10000 by 10000. If the number of TLSs in each composite is increased to 30, the matrix size will accordingly increase to 30000 by 30000. Thus, we need to limit the size of the material to make the computation feasible. The disk is illuminated by a x-polarized Gaussian beam. The incident field is given by

$$\mathbf{E}_0(x,y,z) = E_0\hat{\mathbf{x}}\frac{w_0}{w(z)}\exp\left[-\frac{x^2+y^2}{w(z)}\right]\exp\left[-i\left(kz + k\frac{r^2}{2R(z)} - \psi(z)\right)\right], \tag{S37}$$

where $w(z) = w_0\sqrt{1 + (z_R/z)^2}$, $\mathrm{R}(z) = z[1 + (z_R/z)^2]$, $\psi(z) = \mathrm{atan}(z/z_R)$ and the Rayleigh range $z_R = \pi w_0^2/\lambda$. The waist radius is $w_0 = 0.5\lambda$ and $\lambda = 550\,\mathrm{nm}$. We plot the spatial distribution of the incident electric field in Fig. S6a. To verify this composite material system is a real "material", it is necessary to plot the spatial distribution of electric field and verify that the scattered field make sense. In Fig. S8b, we plot the spatial distributions of its *x* and *y* components and the patterns of the spatial distributions is reasonable. Then, the Farady ratation angle can be obtained by calculating the polarization of the forward scattering wave, which is plotted in Fig. S8d. Furthermore, to clearly demonstrate the bandwidth broadening effect from the nanoparticles, we calcualte the spectra of Farady rotation for the composite material, which is plotted in Fig. S8e.

Reference

[1] Fu, H., Yan, Z., Lee, S. K., & Mansuripur, M. Dielectric tensor characterization and evaluation of several magneto□optical recording media. *J. Appl. Phys.* **78**, 4076-4090 (1995).

[2] Jain, P. K., Xiao, Y., Walsworth, R. & Cohen, A. E. Surface plasmon resonance enhanced magneto-optics (SuPREMO): Faraday rotation enhancement in gold-coated iron oxide nanocrystals. *Nano Lett.* **9**, 1644-1650 (2009).

[3] Wang, L. *et al.* Plasmonics and enhanced magneto-optics in core−shell Co−Ag nanoparticles. *Nano Lett.* **11**, 1237-1240 (2011).

[4] Rinaldi, R. *et al.* Zeeman effect in parabolic quantum dots. *Phys. Rev. Lett*. **77**, 342 (1996).

[5] Claro, F. Spectrum of tight binding electrons in a square lattice with magnetic field. *Physica Status Solidi (b)* ***104***, (1981).

[6] Bennett, H. S., & Stern, E. A. Faraday effect in solids. *Phys. Rev.* **137**, A448 (1965).

[7] Roth, L. M. Theory of the Faraday effect in solids. *Phys. Rev.* **133**, A542 (1964).

[8] Knöll, L., Scheel, S. & Welsch, D.-G. in *Coherence and Statistics of Photons and Atoms* edited by J. Perina (Wiley, New York, 2001).

[9] Chen, X. W., Sandoghdar, V. & Agio, M. Coherent interaction of light with a metallic structure coupled to a single quantum emitter: from superabsorption to cloaking. *Phys. Rev. Lett*. **110**, 153605 (2013).

[10] Yu, Z., Veronis, G., Wang, Z., & Fan, S. One-way electromagnetic waveguide formed at the interface between a plasmonic metal under a static magnetic field and a photonic crystal. *Phys. Rev. Lett.* **100**, 023902 (2008).

[11] Kelly, K. L, Coronado, E., Zhao, L. L. & Schatz, G. C. The optical properties of metal nanoparticles: the influence of size, shape, and dielectric environment. *J. Phys. Chem.: B* **107**, 668-677 (2003).

[12] Chaumet, P. C., Rahmani, A., de Fornel, F. & Dufour, J. P. Evanescent light scattering: The validity of the dipole approximation. *Phys. Rev. B* **58**, 2310 (1998).

[13] Pershan, P. S. Magneto-optical effects. *Journal of Applied Physics **38***, 1482-1490 (1967).

[14] Wubs, M., Suttorp, L.G. & Lagendijk A. Multiple-scattering approach to interatomic interactions and superradiance in inhomogeneous dielectrics. *Phys. Rev. A* **70**, 053823 (2004).

[15] Leistikow, M. D., Johansen, J., Kettelarij, A. J., Lodahl, P. & Vos, W. L. Size-dependent oscillator strength and quantum efficiency of CdSe quantum dots controlled via the local density of states. *Phys. Rev. B* **79**, 045301 (2009).

[16] Stobbe, S., Johansen, J., Kristensen, P. T., Hvam, J. M. & Lodahl, P. Frequency dependence of the radiative decay rate of excitons in self-assembled quantum dots: Experiment and theory. *Phys. Rev. B*. **80**,155307 (2009).

[17] Brokmann, X., Coolen, L., Dahan, M. & Hermier, J. P. Measurement of the radiative and nonradiative decay rates of single CdSe nanocrystals through a controlled modification of their spontaneous emission. *Phys.Rev. Lett*. **93**, 107403 (2004).

[18] Mortensen, N. A., Raza, S., Wubs, M., Søndergaard, T. & Bozhevolnyi, S. I. A generalized non-local optical response theory for plasmonic nanostructures. *Nat. Communications* **5**, 3809 (2014).

[19] Raza, S., Stenger, N., Kadkhodazadeh, S., Fischer, S. V., Kostesha, N., Jauho, A. P., Burrows, A., Wubs, M. & Mortensen, N. A. Blueshift of the surface plasmon resonance in silver nanoparticles studied with EELS. *Nanophotonics* **2**, 131-138 (2013).

[20] Collett, E. *Field guide to polarization*. Bellingham: SPIE press (2005).